ARTICLE

A thermally/chemically robust and easily regenerable anilato-based ultramicroporous 3D MOF for CO_2 uptake and separation

Received 00th January 20xx,
Accepted 00th January 20xx

DOI: 10.1039/x0xx00000x

Noemi Monni,[a,b] Eduardo Andres-Garcia,[b] Katia Caamaño,[b] Víctor García-López,[b] Juan Modesto Clemente-Juan,[b] Mónica Giménez-Marqués,[b] Mariangela Oggianu,[a] Enzo Cadoni,[a] Guillermo Mínguez Espallargas,*[b] Miguel Clemente-León,*[b] Maria Laura Mercuri*[a] and Eugenio Coronado[b]

The combination of the properly designed organic linker, 3,6-N-ditriazoyil-2,5-dihydroxy-1,4-benzoquinone (trz_2An), with Co^{II} ions results in a novel 3D ultramicroporous MOF with high CO_2 uptake capacity and separation efficiency, with particular attention to CO_2/N_2 and CO_2/CH_4 gas mixtures. This material consists of 1D chains of octahedrally coordinated Co^{II} ions linked through the anilato ligands in the equatorial positions and to the triazole substituents from two neighbouring chains in the two axial positions. This leads to a 3D microporous structure with voids with an affinity for CO_2 molecules and channels that enable the selective entrance of CO_2 but not of molecules with larger kinetic diameter such as N_2 or CH_4. The adsorption studies revealed that *i)* the MOF presents a remarkable carbon dioxide uptake, above 20% in weight; *ii)* CO_2 adsorptive separation is successfully performed in CO_2:N_2 and CO_2:CH_4 gas mixtures, exhibiting high selectivity in a large operation range; *iii)* regeneration is easily achieved at mild conditions.

Introduction

Methane (CH_4) has a widespread use as clean energy source, but current natural gas reserves are too contaminated to be considered economically profit-making[1] and the most important contaminants, as CO_2, need to be removed before further transport for processing.[2] Thus, among the hundreds of billions of cubic meters of natural gas produced, approximately 20% requires significant treatments in order to remove CO_2.[3] In addition, capturing CO_2 from the atmosphere represents the key challenge of this century, since CO_2 has been recognized as the primary anthropogenic greenhouse contributor to the increase of earth's average temperature.[4,5] This *Kyoto protocol* gas[6] has been increasing its concentration since industrial revolution, reaching the current alarming level of 415 ppm[7]. Furthermore, separation processes consume upon 70% of the energy cost in typical chemical plant,[8] thus, the importance of separation techniques development research is worldwide acknowledged.[9]

Among the different types of porous materials that can be used for the aforementioned issues, Metal-Organic Frameworks (MOFs) are very versatile networks formed by organic molecules (*linkers*) and metal ions (*nodes*) which self-assemble in a large variety of porous architectures.[10,11] Because of their intrinsic porosity they have attracted ever-growing interest in several applications ranging from gas storage and separation, catalysis, chemical sensing, to biomedicine.[12–15] Noteworthy Long. *et al.* recently reported on the unprecedented adsorption behaviour shown by diamine-appended MOFs, which maintain affinity for CO_2 under moisture exposure and show excellent long-term stability, both crucial requirements for CO_2 capture.[4] Additionally decreasing pore size in ultramicroporous materials (pore size < 0.7 nm), is a remarkable strategy for highly selective sorption properties with benchmark results for CO_2:N_2 separation.[16–18] An alternative strategy consists in the construction of coordination polymers formed by discrete compartments, *i.e.* compartmentalized, featuring internal cavities where small gas molecules can diffuse onto, establishing weak interactions with the network.[19,20] Furthermore, MOFs have the potential to exhibit lower regeneration energies than traditional adsorbents or amine-based solvents. Therefore, they are considered excellent candidates for gas adsorptive separation industrial processes, with particular attention to CO_2 removal from CO_2:CH_4 mixtures, and carbon dioxide capture from air (CO_2:N_2).

Among the linkers, interest has recently been renovated[21–26] on 3,6-disubstituted (X)-2,5-dihydroxybenzoquinone derivatives (X=H, F, Cl, Br, I, CN), *i.e.* anilates, for their ability to act as suitable building blocks of coordination polymers and MOFs, showing peculiar physical properties ranging from layered magnets to magnetic conductors and lanthanide-based 2D NIR-emitters.[27–30] Interestingly, Robson *et al*. have reported on the capability of 1D frameworks of Mg(II) or Zn(II) metal ions to uptake, upon dehydration, significant amounts of H_2, CO_2 and CH_4 at low pressures.[31] Significant amounts of CO_2 are also captured on $(NEt_4)_2[Zn_2(CA)_3]$ and $(NEt_4)_2[Zn_2(FA)_3]$ (CA = chloranilate, FA = fluoranilate) 2D porous compounds.[32] Very recently, uptake of proper sized guest molecules on the porous 2D square-grid framework, $(NEt_4)[Y(CA)_2]$, has been reported, showing high sorption enthalpies for H_2, N_2, CO_2 and, particularly, CH_4 that have been related to the ability of these molecules to interact simultaneously with more than one internal surface of the square channels.[33] However, selective adsorption properties have not been reported for this family of compounds until now.

We herein report on the use of 3,6-N-ditriazoyil-2,5-dihydroxy-1,4-benzoquinone (trz_2An),[34] shown in scheme 1, bearing two triazole

[a] Dipartimento di Scienze Chimiche e Geologiche, Università degli Studi di Cagliari, I-09042 Monserrato, Italy.
[b] Instituto de Ciencia Molecular, Universidad de Valencia, Catedrático José Beltrán 2, 46980 Paterna, Spain.

† Footnotes relating to the title and/or authors should appear here.
Electronic Supplementary Information (ESI) available: [details of any supplementary information available should be included here]. See DOI: 10.1039/x0xx00000x

pendant arms at the 3,6 position of the anilato moiety instead of the much simpler substituents found in this position with a few exceptions.[35] This anilato linker has the potential to construct 3D MOFs, due to the coordinative properties of the N4 atoms of the triazole group.[36] In addition to this, the presence of not coordinated N2 atom and the fact that anilato ring is the most electron-rich among anilates, due to the strong electron-donor power of the triazole group, could enhance the sorption of CO_2 molecules.

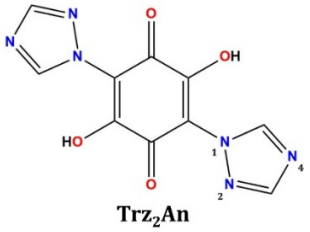

Scheme 1. Chemical structure of the 3,6-N-ditriazoyil-2,5-dihydroxy-1,4-benzoquinone (trz_2An) ligand, indicating the numbered positions of nitrogen in triazole pendant ring.

Results and discussion

By combining $CoCl_2{\cdot}6H_2O$ with trz_2An, in 1:1 stoichiometric ratio, *via* hydrothermal method (**Scheme S1†**), dark brown rectangular crystals of $[Co(trz_2An)]_n{\cdot}3H_2O$ (**1**) suitable for a single crystal X-ray study, were obtained. Remarkably the synthesis of this MOF can be scaled up to 8 times in a proper autoclave (see experimental section).

Crystal Structure

1 crystallizes in the orthorhombic *Pnnm* space group and its asymmetric unit is formed by one Co^{II} ion with an occupancy of 0.25 and one quarter of trz_2An^{2-} ligand plus disordered water molecules. Co^{II} ions are equatorially coordinated to four oxygen atoms of two bis(bidentate) trz_2An^{2-} ligands leading to $[Co(trz_2An)]_n$ chains running along the *c* axis (see **Fig. 1a**). The distorted octahedral coordination sphere of Co^{II} ions is completed with two nitrogen atoms from N4 atoms of the 1,2,4-triazole substituted pendant rings of trz_2An^{2-} ligands from two neighbouring chains. In addition, the bis(bidentate) trz_2An^{2-} ligands of each chain are linked to other two neighbouring chains through N4 atoms of the 1,2,4-triazole substituted pendant rings (**Fig. 1b**), leading to a 3D neutral polymeric framework. The space between four interconnected chains contains pockets, which could be suitable for the sorption of small molecules as CO_2 (**Fig. 1c**). Thus, two voids of 90.4 $Å^3$ were found in the unit cell of the crystals, giving a void volume of 23.5%, which are each occupied in the as-synthetized material by approximately one water molecule. Thermogravimetric analysis (TGA) confirms the presence of water molecules in the channels, which can be removed at 70 ºC with retention of the crystallinity (**Fig. S5†**). TGA also evidences that the dehydrated compound starts to decompose above 400 ºC (**Figs. S8†**). Therefore, variable temperature powder X-ray diffraction (PXRD) measurements, were performed, showing that the observed crystallinity is retained up to 300°C (**Fig. S6†**). Additionally, **1** presents extraordinary chemical stability in aqueous solution retaining its crystallinity under pH values ranging from 1 to 12 **(Figure S7†)**. Magnetic measurements are consistent to that expected for Co^{II} ions with weak antiferromagnetic interactions (**Fig. S9†**) as observed in a 1D compound with two axial water solvent molecules and CA linkers $[Co(CA)(H_2O)_2]{\cdot}G$.[37]

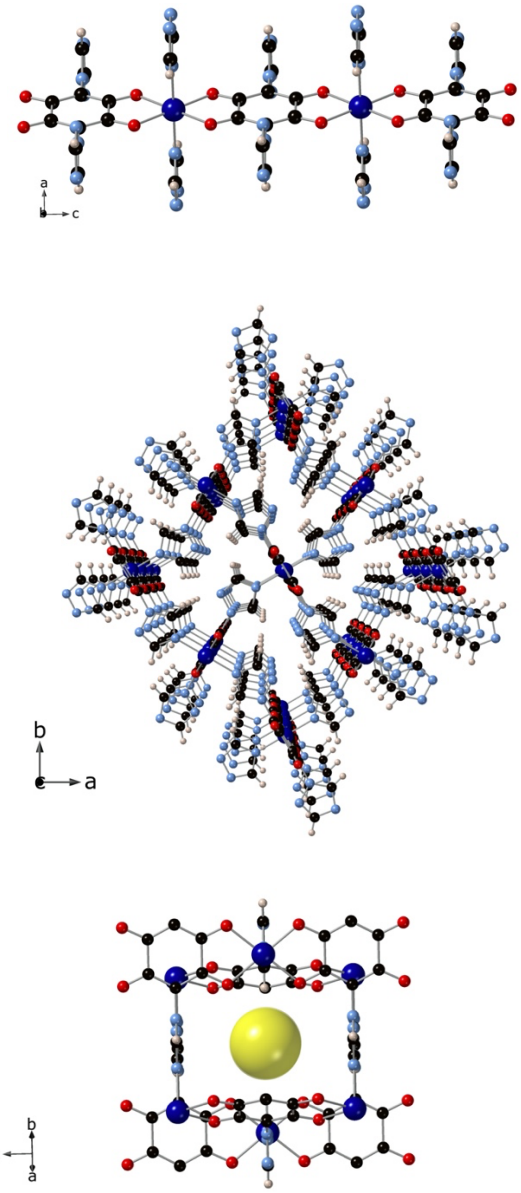

Fig. 1 Crystal structure of **1** showing (a) the anilato-based chains, (b) the microporous channels parallel to the *c*-axis and (c) orthogonal to the *c*-axis with a yellow ball of 4 Å diameter representing the 23.5 % void volume. The black, pink, blue, red, and dark blue spheres represent the C, H, N, O, and Co atoms, respectively.

Static Isothermal Adsorption Measurements

The sorption capacity of activated **1** has been examined with a high pressure gravimetric analyzer. **Fig. 2a** exhibits the remarkably different (high-pressure) adsorption profiles for CO_2, N_2, and CH_4. These gravimetric isotherms reveal the dominant role of kinetics, as the slightly shorter CO_2 kinetic diameter enables its diffusion along the channels of the MOF, reaching a competitive adsorption capacity of 88 ml CO_2 per gram of sample and with BET surface area and Langmuir surface area values of 431 $m^2\ g^{-1}$ and 446 $m^2\ g^{-1}$, respectively (Fig. S9†). An outstanding CO_2 adsorption capacity[38] is found for **1**, with more than 20% in weight (5.4 mmol g^{-1}, at 10 bar and 298 K), while nitrogen and methane values are negligible (even at high pressure). Variable temperature measurements show the expected increase in adsorbed CO_2 with decreasing temperature

(**Fig. 2b**), allowing the calculation of the adsorption enthalpy to be 21.07 kJ mol^{-1} (**Fig. S12†**), in agreement with typical interaction of CO_2 with triazole groups.[39] Kinetics analysis reveals a second effect with temperature, as adsorption is noticeably faster in low pressure region at low temperature (**Fig. S11†**). That facility of reaching equilibrium is of outmost importance for industrial implementation, as it favours the use of the MOF in dynamic conditions.

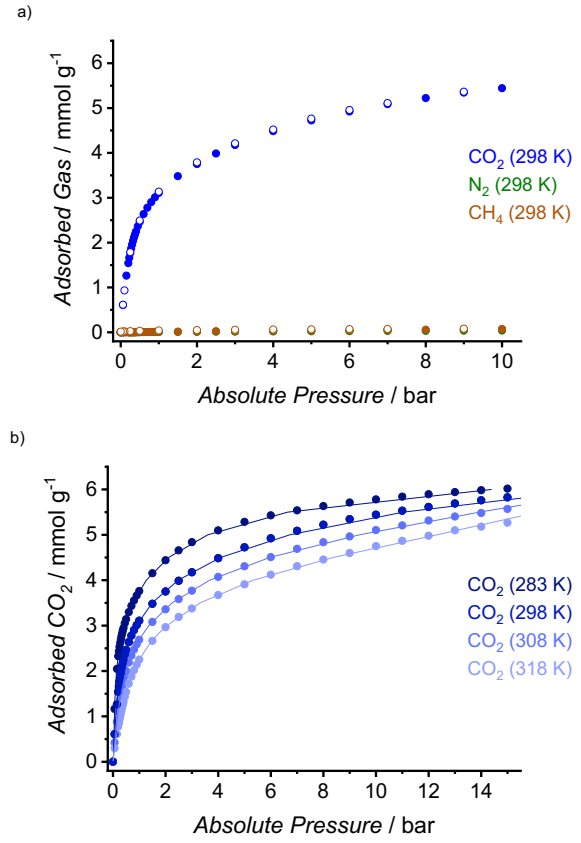

Fig. 2. High pressure gravimetric single-gas isotherms for **1**: *a*) CO_2 (*blue*), N_2 (*green*) and CH_4 (*orange*) gas adsorption isotherms on **1**, at 298 K; *b*) CO_2 gas adsorption isotherms on **1**, at different temperatures (283 K – 318 K), including Virial fittings. Solid circles for adsorption and open ones for desorption.

Dynamic Adsorptive Separation Measurements

Dynamic condition measurements in a Breakthrough setup mimic the behaviour of the MOF in a real gas adsorptive separation process. In **Fig. 3**, breakthrough profiles for separation of 1:4 (CO_2:N_2 and CO_2:CH_4) mixtures are reported (further measurements with different mixture compositions can be found in the Supporting Information, section **S6b†**). The outlet flow is analysed after breaking through the column, exhibiting both an outstanding adsorption region for CO_2, and an overlapping between the tracer curve and the second gas in the mixture.

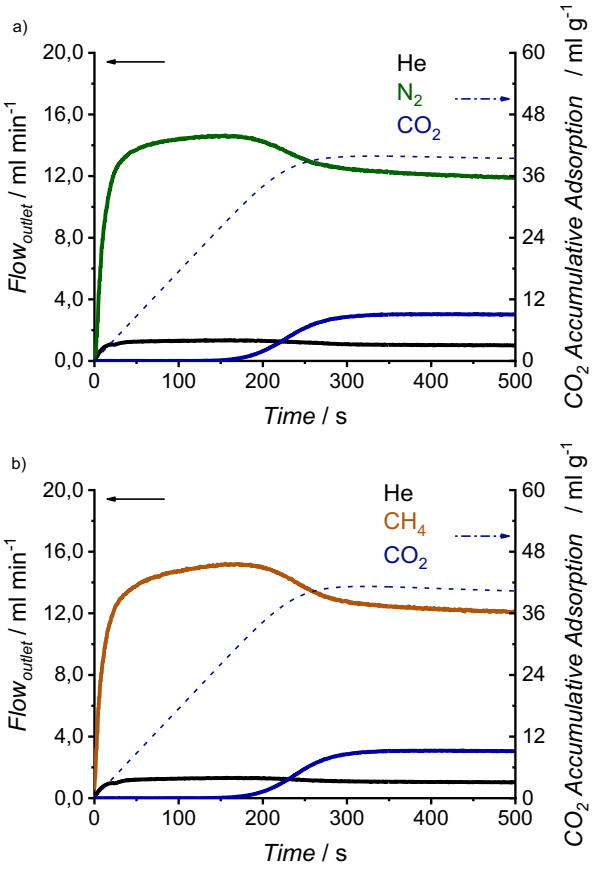

Fig. 3. Breakthrough exit flowrates (solid line, left axis) and CO_2 accumulative adsorption (dash-dot line, right axis) vs. time at 283 K and 1 bar, on **1**. Inlet composition corresponds to a 20 % dilution of CO_2: *a*) in nitrogen, and *b*) in methane. Time zero is set with the first detection of helium (tracer). The total flow rate is 15 ml min^{-1}.

In **Fig. 4** the experimental results from the breakthrough measurements are summarized, performed for two gas mixtures (CO_2:N_2 and CO_2:CH_4), three temperatures (283 K, 298 K and 323 K) and three CO_2 inlet concentrations (5 %, 20 % and 50 %). As adsorption is an exothermic process, it is promoted at low temperature, in concordance with the obtained results. Initial analysis of these results indicates that the adsorption capacity decrease with lowering CO_2 concentration and increasing temperature.

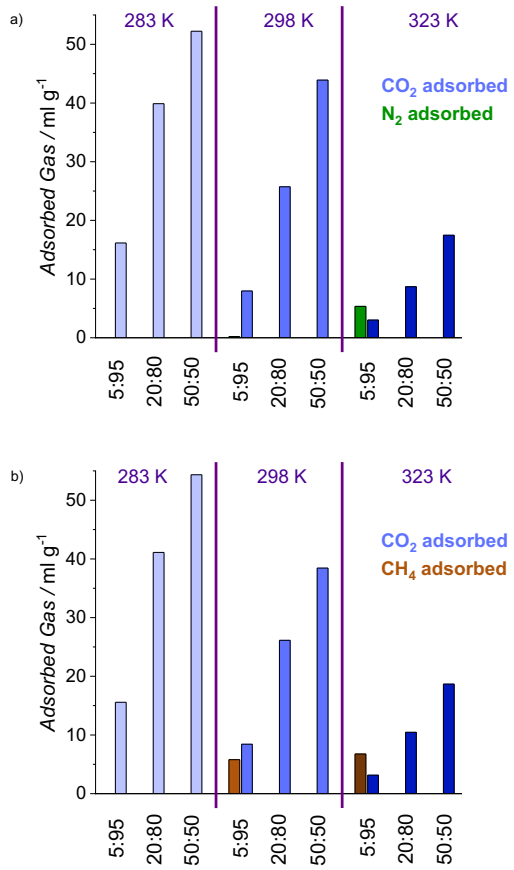

Fig. 4. Gas adsorbed amounts on **1**, calculated from breakthrough profiles, at 1 bar (absolute pressure) for: *a*) CO_2:N_2, and *b*) CO_2:CH_4 mixtures; at different concentrations (5 %, 20 % and 50 %) and different temperatures (283 K, 298 K and 323 K). Time zero is set with the first detection of helium (tracer).

A more in-depth analysis of the capacity of the material to discriminate between the gases can be obtained by analysing the selectivity, α (Table 1). As it can be observed in Table 1, **1** exhibits the same trends and capacities/selectivity ranges for both CO_2:N_2 and CO_2:CH_4 mixtures, with very large selectivity values (α > 1000) obtained in all the ranges of temperature and composition. In fact, even at the most critical conditions (low CO_2 concentration and high temperature), the selectivity values still are significantly large (α = 10), being among the best MOFs reported so far. At similar conditions, ZIF-95 and ZIF-100 have α values in the range 4 to 25,[40] amino-functionalized MIL-53, (NH_2)-MIL-53(Al), presents α values in the range 20 to 200,[41] the compartmentalized coordination polymer CCP-6 have α values in the range 3 to >1000 (only at most favoured conditions),[19] and a novel L-histidine-based 3D chiral MOF, Cu^{II} 2(S,S)- hismox·$5H_2O$, has also been shown to be very effective, with α values above 1000, in kinetics-controlled separation processes.[42] In addition, a further advantage of **1** is its high capacity, which is competitive with effective CO_2 capture materials, as MOF-74(Me),[43] HHU-2[44] or some *rh*t-type MOFs.[45] But more importantly, fully regeneration of **1** is achieved at room temperature and ambient pressure , by simply flowing argon for 20 minutes (see **Figs. S21-S22†** and **Tables S4-S5†** in Supplementary Material, where the double replicas of the breakthrough measurements are plotted for comparison).

Table 1. Experimental dynamic selectivities (α)[a] for **1**; calculated from the integration of the breakthrough curves, considering gas mixture inlet composition.

	5% CO_2 (in N_2 mixture)	20% CO_2 (in N_2 mixture)	50% CO_2 (in N_2 mixture)
283 K	>1000	>1000	>1000
298 K	>500	>1000	>1000
323 K	10	>1000	>1000
	5% CO_2 (in CH_4 mixture)	20% CO_2 (in CH_4 mixture)	50% CO_2 (in CH_4 mixture)
283 K	>1000	>1000	>1000
298 K	26	>1000	>1000
323 K	8	>1000	>1000

[a] $\alpha = [(q_{ads,1}/F_{0,1})/(q_{ads,2}/F_{0,2})]$, where $q_{ads,i}$ represents the gas adsorbed amount, and $F_{0,i}$ the inlet single-gas flow, for carbon dioxide (1) and the secondary gas (2).

Conclusions

The trz_2An anilate derivative, bearing a triazole pendant arm at the 3,6 position of the anilato moiety, has been used for the first time in combination with Co^{II} nodes to afford **1**, a 3D MOF formed by 1D chains of octahedrally coordinated Co^{II} ions linked through the anilato ligands. Interestingly, the two axial positions of Co^{II} in these chains are bridged by the triazole substituents from two neighbouring chains, which act as ancillary groups, instead of the solvent molecules, commonly found in similar compounds reported in the literature. This leads to a very stable and robust 3D ultramicroporous structure with channels to enable the selective entrance of CO_2, hindering the diffusion of molecules with larger kinetic diameter, such as N_2 or CH_4. The presence of triazole rings in the structural voids increases the affinity for CO_2 molecules. In order to evaluate the potential of this MOF in adsorptive separations, static and dynamic adsorption measurements were performed. Although competitors in CO_2 adsorption are reported in the literature,[44,45] MOF **1** presents not only high adsorption static capacity (above 20% in weight), but also approaching values at dynamic conditions and an outstanding selectivity in both nitrogen and methane mixtures. It should be noted that a good CO_2 sorption capacity is not enough for a material to serve for separation applications, if the CO_2 is not adsorbed selectively. MOF **1**, which shows peculiar thermal and chemical robustness, is presented as a promising alternative in CO_2 gas separation processes, since it combines the advantages from both kinetic and thermodynamic control mechanisms. Remarkably, its framework is able to sieve larger molecules, as nitrogen or methane, to reach outstanding CO_2 selectivity values (>1000), at different temperature and concentration conditions. Remarkably, the material can be regenerated at mild conditions. The favourable balance of these three characteristics *i.e.* high selectivity, high adsorption capacity and high regenerability, positions **1** as an exceptional candidate in separation technology industry.

Experimental section

Trz_2An was prepared according to the literature.[34] Reagents of analytical grade were purchased from Zentek (TCI) and Sigma Aldrich and used without further purification. Elemental analyses (C, H, and N) were performed with a CE Instruments EA 1110 CHNS. FT-IR spectra were performed in KBr pellets in a Bruker Equinox 55 spectrophotometer. TGA was performed in alumina crucibles with

the instrument STA-6000 under nitrogen flux (40 mL/min), in the 25-800°C temperature range at 10°C/min. PXRD patterns were performed using a 0.7 mm glass capillary filled with polycrystalline samples of the compounds and mounted and aligned on an Empyrean PANalytical powder diffractometer, using Cu Kα radiation (λ = 1.541 77 Å). A total of three scans were collected for each compound at room temperature in the 2θ range of 10–40°. Variable-temperature PXRD patterns were measured in a θ–θ Bragg–Brentano focalizing geometry Bruker D8 Avance A25 diffraction system equipped with a Cu Kα source (λ = 1.54056 Å), in the 2θ range of 2–40° and in the temperature range 25-400°C. Magnetic measurements were performed with a Quantum Design MPMS-XL-5 SQUID magnetometer in the 2–300 K temperature range with an applied magnetic field of 0.1 T at a scan rate of 2 K min^{-1}.

Synthesis of $[Co(trz_2An)]_n \cdot 3H_2O$ (1). A 5 mL Teflon vial with a mixture of $CoCl_2 \cdot 6H_2O$ (11.9 mg, 0.05 mmol), trz_2An (13.7 mg, 0.05 mmol), NaOH (4 mg, 0.1 mmol) and water (5 mL) was heated at 130°C for 48 hours. After being cooled to room temperature, rectangular dark brown crystals, suitable for an X-ray diffraction study, were obtained. To obtain a large quantity of **1**, the synthesis was performed in a stainless steel autoclave of 80 mL volume, with a scale up of the reaction mixture of 8 times, by using 0.4 mmol of trz_2An, 0.8 mmol of NaOH and 0.4 mmol of $CoCl_2 \cdot 6H_2O$ in 40 mL of water. Elemental Analysis: *Calcd %* for $C_{10}H_{10}N_6O_7Co$ (385.16): C, 31.18; H, 2.62; N, 21.82. *Found:* C, 31.12; H, 2.45; N, 22.00.

Structure of 1

A single crystal of **1** was mounted on a glass fiber using a viscous hydrocarbon oil to coat the crystal and then transferred directly to the cold nitrogen stream for data collection. X-ray data of 1 were collected at 120 K on a Supernova diffractometer equipped with a graphite-monochromated Enhance (Mo) X-ray Source (λ = 0.710 73 Å). The program CrysAlisPro, Oxford Diffraction Ltd., was used for unit cell determinations and data reduction. Empirical absorption correction was performed using spherical harmonics, implemented in the SCALE3 ABSPACK scaling algorithm. The structures were solved with the ShelXT structure solution program[46] and refined with the SHELXL-2013 program,[47] using Olex2.[48] Non-hydrogen atoms were refined anisotropically, and hydrogen atoms were placed in calculated positions refined using idealized geometries (riding model) and assigned fixed isotropic displacement parameters. Crystallographic data are summarized in Table S2. CCDC-2091526 contains the supplementary crystallographic data for this paper.

Gas sorption

Low pressure nitrogen and carbon dioxide volumetric isotherms were carried out in a Tristar II Plus Micromeritics sorptometer, at 77 K and 273 K, respectively. Activation was set at 393 K, under vacuum, for 2 hours. High-pressure gravimetric adsorption isotherms of CO_2, CH_4 and N_2 were measured at different temperatures, ranging from 283 to 318 K, in an IGA-100 gas sorption analyser (from Hiden Isochema) using approximately 50 mg of sample. Before each adsorption experiment, the sample was outgassed at 393 K under vacuum (10^{-5} Pa) for two hours. Equilibrium conditions corresponded to 600 s interval, and 0.001 mg min^{-1} tolerance.

Dynamic Adsorptive Separation Measurements

An ABR (HIDEN Isochema) automated breakthrough analyser setup, based on a packed adsorption column, was used to determine the adsorption dynamics of gas mixtures. Pressure, temperature and inlet composition are controlled, and the outlet composition is analysed, by an integrated mass spectrometer (HPR-20 QIC). The fixed-bed column was filled with 286 mg of compound **1**. Before each measurement, the sample was regenerated at atmospheric temperature and pressure, in 40 ml min^{-1} Ar flow for 20 minutes. Operation conditions ranged 283-323 K, at 1 bar. The inlet mixture was set to a 15 ml min^{-1} flow of a dilution of carbon dioxide in N_2 or CH_4 (5%, 20%, 50%). Time zero was set with the first detection of helium, which was used as a trace (an extra 1 ml min^{-1} of He in the total feed flow of 16 ml min^{-1}).

Conflicts of interest

There are no conflicts to declare.

Author Contributions

MLM and NM designed the MOF. MLM, EC and MCL directed the research project. NM synthesized the MOF under the supervision of MLM and EC while it has been characterized with the help of VGL and the supervision of MCL. JMCJ performed the theoretical modelling of the magnetic measurements. EAG and KC performed gas sorption experiments and analyzed the data under the supervision of GME and MGM. MLM, MCL and GME wrote the manuscript. All authors contributed to the final interpretation of the experimental results and critically revised the manuscript. All authors have read and approved the final version of the manuscript.

Acknowledgements

Fondazione di Sardegna - Convenzione triennale tra la Fondazione di Sardegna e gli Atenei Sardi, Regione Sardegna - L.R. 7/2007 annualità 2018 - DGR 28/21 del 17.05.2015, through project F74I19000940007 is acknowledged for financial support. CESA (Centro d'Eccellenza per la Sostenibilità Ambientale, accordo di programma RAS-UNICA-IGEA-AUSI, project number E58C16000080003) and MIUR (Ministry of Education, University, Research) UNICA-UNISS Consortium PhD Course on Chemical Sciences and Technologies, are also acknowledged for the PhD grant of MO and NM. Financial support from the EU (ERC Advanced Grant MOL-2D 788222, ERC Consolidator Grant S-CAGE 724681, FET-OPEN COSMICS 766726 and COST action MOLSPIN CA15128), the Spanish MICINN (PID2020-118564GA-I00, PID2020-117264GB-I00, PID2020-117177GB-I00, and Unidad de Excelencia María de Maeztu CEX2019-000919-M), the Generalitat Valenciana (PROMETEO program and iDiFEDER/2018/061) and the Ministry of Education and Science of Russian Federation (Agreement No.14.W03.31.0001) is gratefully acknowledged. MGM, EAG and KC thank MICINN for a "Ramón y Cajal" (RYC2019-027902-I), a "Juan de la Cierva Formación" (FJC2019-039015-I) and a predoctoral (PRE2018-08335) fellowships, respectively. Variable temperature PXRD was performed in the facility of SCSIE Univ. of Valencia. We all thank A. M. Mestre-Segarra, A. Soriano-Portillo, J. M. Martínez-Agudo and G. Agustí for PXRD and magnetic measurements.

Notes and references

1 R. van Wissen, M. Golombok and J. J. H. Brouwers, *Separation of carbon dioxide and methane in continuous countercurrent gas centrifuges*, 2005, vol. 60.

2 K. Liao, Q. Yao, X. Wu and W. Jia, *Energies*, 2012, **5**, 3892–3907.

3 R. W. Baker, *Membrane technologies and applications*, John Wiley & Sons, Ltd, 2nd editio., 2011.

4 R. Hughes, G. Kotamreddy, A. Ostace, D. Bhattacharyya, R. L. Siegelman, S. T. Parker, S. A. Didas, J. R. Long, B. Omell and M. Matuszewski, *Energy & Fuels*, 2021, **35**, 6040–6055.

5 R. L. Siegelman, E. J. Kim and J. R. Long, *Nat. Mater.*, 2021, **20**, 1060–1072.

6 C. Cambridge University Press UK, *IPCC, 2007: Summary for Policymakers. In: Climate Change 2007: ThePhysical Science Basis*, 2007.

7 H. Yang, Z. Xu, M. Fan, R. Gupta, R. B. Slimane, A. E. Bland and I. Wright, *J. Environ. Sci.*, 2008, **20**, 14–27.

8 P. C. Wankat, *Separation Process Engineering: includes mass transfer analysis. (4th ed.)*, Prentice Hall, Massachusetts (USA), 2017.

9 D. S. Sholl and R. P. Lively, *Nature*, 2016, **532**, 435–437.

10 H.-C. Zhou, J. R. Long and O. M. Yaghi, *Chem. Rev.*, 2012, **112**, 673–674.

11 H.-C. J. Zhou and S. Kitagawa, *Chem. Soc. Rev.*, 2014, **43**, 5415–5418.

12 H. Li, K. Wang, Y. Sun, C. T. Lollar, J. Li and H. C. Zhou, *Mater. Today*, 2018, **21**, 108–121.

13 V. Pascanu, G. González Miera, A. K. Inge and B. Martín-Matute, *J. Am. Chem. Soc.*, 2019, **141**, 7223–7234.

14 S. A. Diamantis, A. Margariti, A. D. Pournara, G. S. Papaefstathiou, M. J. Manos and T. Lazarides, *Inorg. Chem. Front.*, 2018, **5**, 1493–1511.

15 M. Oggianu, N. Monni, V. Mameli, C. Cannas, S. A. Sahadevan and M. L. Mercuri, *Magnetochemistry*, 2020, **6**, 1–14.

16 P. M. Bhatt, Y. Belmabkhout, A. Cadiau, K. Adil, O. Shekhah, A. Shkurenko, L. J. Barbour and M. Eddaoudi, *J. Am. Chem. Soc.*, 2016, **138**, 9301–9307.

17 K. J. Chen, D. G. Madden, T. Pham, K. A. Forrest, A. Kumar, Q. Y. Yang, W. Xue, B. Space, J. J. Perry, J. P. Zhang, X. M. Chen and M. J. Zaworotko, *Angew. Chem. Int. Ed.*, 2016, **55**, 10268–10272.

18 S. Mukherjee, S. Chen, A. A. Bezrukov, M. Mostrom, V. V. Terskikh, D. Franz, S. Q. Wang, A. Kumar, M. Chen, B. Space, Y. Huang and M. J. Zaworotko, *Angew. Chem. Int. Ed.*, 2020, **59**, 16188–16194.

19 G. Mínguez Espallargas, E. Miguel-Casañ, E. Andres-Garcia, J. Calbo and M. Giménez-Marqués, *Chem. Eur. J.*, 2021, **27**, 4653-4659

20 M. Giménez-Marqués, N. Calvo Galve, M. Palomino, S. Valencia, F. Rey, G. Sastre, I. J. Vitórica-Yrezábal, M. Jiménez-Ruiz, J. A. Rodríguez-Velamazán, M. A. González, J. L. Jordá, E. Coronado and G. M. Espallargas, *Chem. Sci.*, 2017, **8**, 3109–3120.

21 L. E. Darago, M. L. Aubrey, C. J. Yu, M. I. Gonzalez and J. R. Long, *J. Am. Chem. Soc.*, 2015, **137**, 15703–15711.

22 S. A. Sahadevan, A. Abhervé, N. Monni, C. Sáenz de Pipaón, J. R. Galán-Mascarós, J. C. Waerenborgh, B. J. C. Vieira, P. Auban-Senzier, S. Pillet, E.-E. Bendeif, P. Alemany, E. Canadell, M. L. Mercuri and N. Avarvari, *J. Am. Chem. Soc.*, 2018, **140**, 12611–12621.

23 S. Ashoka Sahadevan, N. Monni, M. Oggianu, A. Abhervé;, D. Marongiu, M. Saba, A. Mura, G. Bongiovanni, V. Mameli, C. Cannas, N. Avarvari, F. Quochi and M. L. Mercuri, *ACS Appl. Nano Mater.*, 2020, **3**, 94-104

24 J. A. DeGayner, I. R. Jeon, L. Sun, M. Dincă and T. D. Harris, *J. Am. Chem. Soc.*, 2017, **139**, 4175–4184.

25 S. Benmansour, A. Hernández-Paredes, A. Mondal, G. López Martínez, J. Canet-Ferrer, S. Konar and C. J. Gómez-García, *Chem. Commun.*, 2020, **56**, 9862–9865.

26 A. E. Thorarinsdottir and T. D. Harris, *Chem. Rev.*, 2020, **120**, 8716–8789.

27 M. L. Mercuri, F. Congiu, G. Concas and S. Ashoka Sahadevan, *Magnetochemistry*, 2017, **3**, 17.

28 M. Atzori, S. Benmansour, G. Mínguez Espallargas, M. Clemente-León, A. Abhervé, P. Gómez-Claramunt, E. Coronado, F. Artizzu, E. Sessini, P. Deplano, A. Serpe, M. L. Mercuri and C. J. Gómez García, *Inorg. Chem.*, 2013, **52**, 10031–10040.

29 S. Benmansour, A. Abhervé, P. Gómez-Claramunt, C. Vallés-García and C. J. Gómez-García, *ACS Appl. Mater. Interfaces*, 2017, **9**, 26210–26218.

30 S. Ashoka Sahadevan, N. Monni, A. Abhervé, D. Marongiu, V. Sarritzu, N. Sestu, M. Saba, A. Mura, G. Bongiovanni, C. Cannas, F. Quochi, N. Avarvari and M. L. Mercuri, *Chem. Mater.*, 2018, **30**, 6575–6586.

31 B. F. Abrahams, A. D. Dharma, B. Dyett, T. A. Hudson, H. Maynard-Casely, C. J. Kingsbury, L. J. Mc Cormick, R. Robson, A. L. Sutton and K. F. White, *Dalton Trans.*, 2016, **45**, 1339–1344.

32 C. J. Kingsbury, B. F. Abrahams, D. M. D'Alessandro, T. A. Hudson, R. Murase, R. Robson and K. F. White, *Cryst. Growth Des.*, 2017, **17**, 1465–1470.

33 C. J. Kingsbury, B. F. Abrahams, J. E. Auckett, H. Chevreau, A. D. Dharma, S. Duyker, Q. He, C. Hua, T. A. Hudson, K. S. Murray, W. Phonsri, V. K. Peterson and R. Robson, *Chem. Eur. J.*, 2019, **25**, 5222–5234.

34 W. Gauβ, H. Heitzer and S. Petersen, *Justus Liebigs Ann. Chem.*, 1973, **764**, 131–144.

35 M. Atzori, F. Pop, T. Cauchy, M. L. Mercuri and N. Avarvari, *Org. Biomol. Chem.*, 2014, **12**, 8752–8763.

36 C. J. Kingsbury, B. F. Abrahams and R. Robson, *CCDC 1568063 Experimental Crystal Structure Determination,* 2017, DOI: 10.5517/ccdc.csd.cc1pmppp

37 S. Kawata, S. Kitagawa, H. Kumagai, T. Ishiyama, K. Honda, H. Tobita, I. Keiichi Adachi and M. Katada, *Chem. Mater.*, 1998, **10**, 3902–3912.

38 R. S. Liu, X. D. Shi, C. T. Wang, Y. Z. Gao, S. Xu, G. P. Hao, S. Chen and A. H. Lu, *ChemSusChem*, 2021, **14**, 1428–1471.

39 Z. Luo, L. Liu, J. Ning, K. Lei, Y. Lu, F. Li and J. Chen, *Angew. Chem. Int. Ed.*, 2018, **57**, 9443–9446.

40 B. Wang, A. P. Cote, H. Furukawa, M. O'Keeffe and O. M. Yaghi, *Nature*, 2008, **453**, 207–211.

41 S. Couck, E. Gobechiya, C. E. A. Kirschhock, P. Serra-Crespo, J. Juan-Alcañiz, A. Martinez Joaristi, E. Stavitski, J. Gascon, F. Kapteijn, G. V Baron and J. F. M. Denayer, *ChemSusChem*, 2012, **5**, 740–750.

42 M. Mon, R. Bruno, E. Tiburcio, A. Grau-Atienza, A. Sepúlveda-Escribano, E. V Ramos-Fernandez, A. Fuoco, E.

Esposito, M. Monteleone, J. C. Jansen, J. Cano, J. Ferrando-Soria, D. Armentano and E. Pardo, *Chem. Mater.*, 2019, **31**, 5856-5866

43 A. C. Kizzie, A. G. Wong-Foy and A. J. Matzger, *Langmuir*, 2011, **27**, 6368–6373.

44 Z. Lu, J. Zhang, J. Duan, L. Du and C. Hang, *J. Mater. Chem. A*, 2017, **5**, 17287–17292.

45 B. Zheng, J. Bai, J. Duan, L. Wojtas and M. J. Zaworotko, *J. Am. Chem. Soc.*, 2011, **133**, 748–751.

46 G. M. Sheldrick, *Acta Crystallogr. Sect. A Found. Crystallogr.*, 2015, **71**, 3–8.

47 G. M. Sheldrick, *Acta Crystallogr. Sect. C Struct. Chem.*, 2015, **71**, 3–8.

48 O. V. Dolomanov, L. J. Bourhis, R. J. Gildea, J. A. K. Howard and H. Puschmann, *J. Appl. Crystallogr.*, 2009, **42**, 339–341.